Active Control of Separation From the Flap of a Supercritical Airfoil

LaTunia Pack Melton* and Chung-Sheng Yao†

Flow Physics and Control Branch

NASA Langley Research Center, Hampton, VA 23681

Avi Seifert ‡

Tel-Aviv University, Ramat-Aviv 69978, ISRAEL

Zero-mass-flux periodic excitation was applied at several regions on a simplified high-lift system to delay the occurrence of flow separation. The NASA Energy Efficient Transport (EET) supercritical airfoil was equipped with a 15% chord simply hinged leading edge flap and a 25% chord simply hinged trailing edge flap. Detailed flow features were measured in an attempt to identify optimal actuator placement. The measurements included steady and unsteady model and tunnel wall pressures, wake surveys, arrays of surface hot-films, flow visualization, and particle image velocimetry (PIV). The current paper describes the application of active separation control at several locations on the deflected trailing edge flap. High frequency ($F^+ \approx 10$) and low frequency amplitude modulation ($F^+_{AM} \approx 1$) of the high frequency excitation were used for control. It was noted that the same performance gains were obtained with amplitude modulation and required only 30% of the momentum input required by pure sine excitation.

*Member, AIAA, l.p.melton@larc.nasa.gov

†c.s.yao@larc.nasa.gov

‡Associate Fellow, AIAA, seifert@eng.tau.ac.il, Senior lecturer, Dept. of Fluid Mechanics and Heat Transfer, School of Mechanical Engineering, Faculty of Engineering. Also, visiting scientist, National Institute of Aerospace, Hampton, VA

I. Nomenclature

c	model chord
C_μ	oscillatory excitation momentum
	coefficient, $\equiv J^{'}/cq$
C_{dp}	pressure drag coefficient
C_D	total drag
C_L	lift coefficient
$C_{L,max}$	maximum lift coefficient
C_p	pressure coefficient, $\equiv (P - P_s)/q$
$C_{p,min}$	minimum pressure coefficient
f	oscillation frequency, Hz
F^+	reduced frequency, $\equiv (f x_{sp})/U_\infty$
h	slot height or width
J'	oscillatory momentum at slot exit, $\equiv \rho h u_j^{'2}$
M	Mach number
P	pressure
P_s	static pressure
q	freestream dynamic pressure,$\equiv 1/2\rho U_\infty^2$
Re_c	chord Reynolds number, $\equiv U_\infty c/\nu$
x_{sp}	distance from actuator to trailing edge
T	temperature
U, u	average and fluctuating streamwise velocity
x/c	normalized streamwise location
z	spanwise location
α	angle of attack
δ_f	TE flap deflection angle
δ_s	LE flap deflection angle
δ^*	boundary layer displacement thickness, $\int_0^\infty (1 - \frac{\rho u}{\rho_e u_e}) dy$
ν	kinematic viscosity
ρ	density

A. Abbreviations

AFC	active flow control
AM	amplitude modulation
BL	boundary layer
LE	leading edge
TE	trailing edge
VSF	vortex shedding frequency

B. Subscripts

j	conditions at excitation slot
S	separation
∞	freestream conditions

C. Superscript

$'$	standard deviation of fluctuating value

II. Introduction

Numerous experiments at both low[1] and high[2,3] Reynolds numbers have shown that periodic excitation is effective as well as efficient at controlling separation. This knowledge combined with the results of a system study,[4] indicating the possibility of significant payoffs such as net airplane cost, weight, and cruise drag reductions, has led to the application of active separation control to a "simplified high-lift system". The purpose of the current investigation is to explore ways to simplify current multi-element high-lift airfoils[5] that use slots and the Fowler effect to generate high-lift. The chosen design completely eliminates hinges and positioning actuators that are external to the airfoil contour as well as passive slots for energizing the boundary layer. All hinges and positioning actuators could be internal, and thus reduce parasitic drag at cruise. The leading edge (LE) flap is used to increase $C_{L,max}$, due to increased circulation and prevention of laminar leading edge separation. Zero-mass-flux periodic excitation, directed downstream at a shallow angle to the local surface, is

applied at locations that are prone to separation, i.e. the LE and trailing edge (TE) flap shoulders.

Flow control research using steady momentum transfer on a high–lift system dates back to the 1930's.[6] Additional interest was spurred in the 1950's by the use of the gas turbine engine. The research showed that separation could be controlled effectively using steady momentum injection but that the momentum requirement was very large.[6] The use of periodic excitation for separation control on the simply hinged high-lift system should reduce the momentum requirements compared to that of steady suction or blowing. In addition, research using pulsed excitation has also shown that the momentum requirements can be reduced further by varying the duty cycle of the excitation.[7]

The results obtained when applying periodic excitation at the LE flap shoulder of this airfoil were reported in a previous publication.[8] High frequency periodic excitation, typical of the piezoelectric actuators currently used, was applied at the LE flap shoulder, and delayed stall and increased $C_{L,max}$ by 10-15%, at low TE flap deflections. It was shown that low frequency amplitude modulation could be used to achieve similar benefits in aerodynamic performance and required 50% -70% less C_μ. In this paper, the effect of introducing periodic excitation on the TE flap, upstream of the turbulent boundary layer separation region is examined.

III. Experiment

Details about the wind tunnel and instrumentation can be found in Ref. 8. Included here are details about the model and actuator used for controlling flow separation on the TE flap.

A. Simplified High–Lift Model

The simplified high-lift version of the NASA EET airfoil[5] was designed in a modular manner so that zero-net mass flux actuators could replace solid regions in the model near the LE and TE flap shoulders (Fig. 1(a)). The 406.4 mm chord model has a 15% chord LE flap that can be deflected from 0^o to -30^o and a 25% chord TE flap that can be deflected from 0^o to 60^o. Angle of attack settings for the airfoil and the two flaps were automated and closed-loop computer controlled. The model has 78 streamwise static pressure taps located at mid span and two rows of 18 spanwise static pressure taps spaced 50.8 mm apart located at x/c = 0.35 and x/c = 0.94 on the upper surface. In addition to the static pressure taps, there are

nine unsteady pressure transducers on the model surface and at least one unsteady pressure transducer embedded in each actuator cavity. The unsteady pressure transducer is used to monitor the pressure fluctuations produced by the actuator and to correlate the wind tunnel experiments with the bench-top actuator calibration tests.

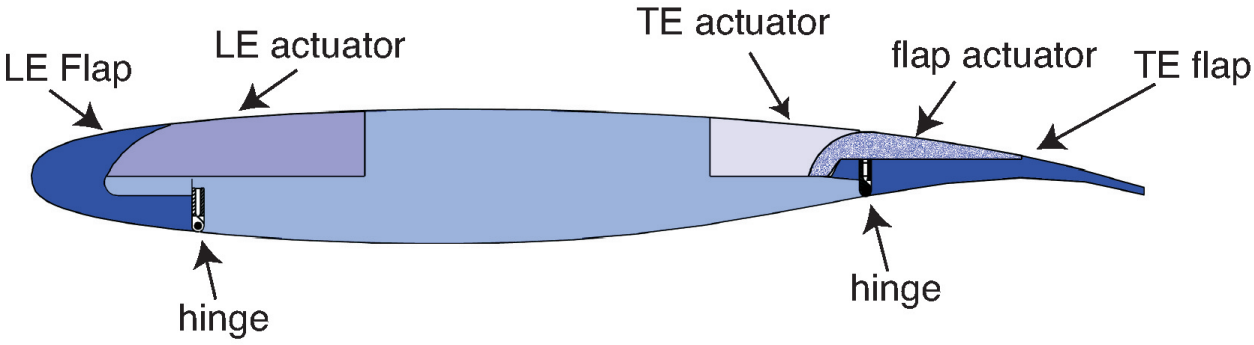

(a) **Actuator regions of EET model.**

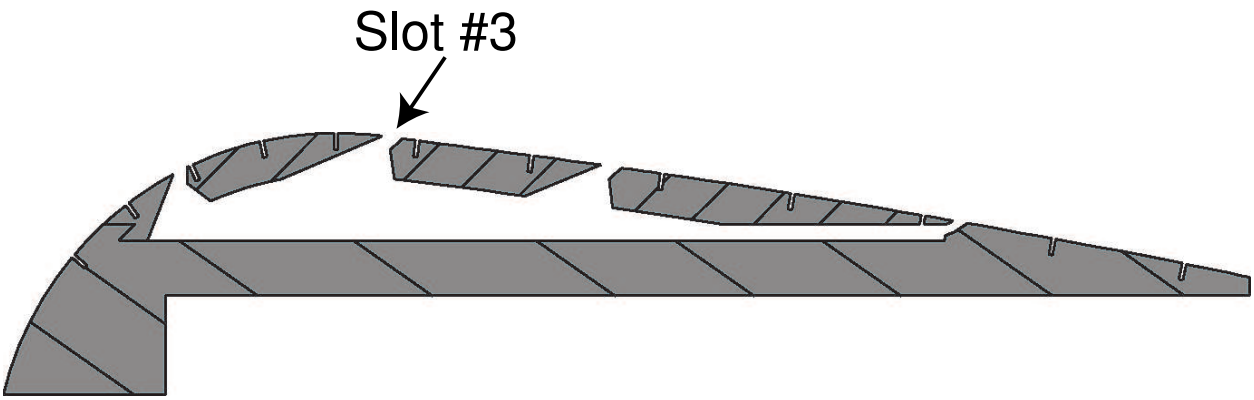

(b) **Flap actuator cross–section.**

Figure 1. Modified EET model

B. Flap Actuator

An internal Piezo-electric actuator was used on the TE flap (Figs. 1). The flap actuator, with its four alternative excitation slots, all inclined at about 30^o to the surface and directed downstream, is shown in Fig. 1(b). The three upstream slots are 0.635 mm wide, and the aft slot is 0.51 mm wide. The x/c locations for the flap actuator slots ($\delta_f = 0^o$) are given in

Table 1.

Table 1. Flap actuator slot locations

Slot	x/c location at $\delta_f = 0^o$
FWD	0.725
#3	0.757
Not Used	0.790
AFT	0.845

The three forward slots are segmented (19 segments, 0.051 m in length) and the aft slot is continuous. A comprehensive bench-top calibration, using a single hot-wire that was traversed along the span of each slot with all other slots sealed, was performed on the flap actuator prior to installation in the tunnel. Unsteady pressures were measured in the actuators cavity to monitor its operation during the calibration and while in the tunnel. The flap actuator was operated at its resonant frequency (1 kHz $\pm$ 0.3 kHz, depending on the slot used) using a pure sine wave and also with an amplitude modulation (AM) at frequencies lower by an order of magnitude than the actuator's resonant frequency. Only one slot was active during each experiment. The three forward slots were sealed using a water-soluble filler to minimize surface discontinuities, and kapton tape, 0.051 mm thick and 12.7 mm wide, was used to seal the aft slot.

C. PIV Set-Up

Two-dimensional digital particle image velocimetry (PIV) was used to measure the instantaneous flow fields, phase synchronized with the flap actuator cycle (when active). The PIV system includes two 1K x 1K cameras installed side by side with 105 mm Macro lens. The fields of view from the two cameras were overlapped to capture the entire TE flap region. The width of the measurement plane was about 120 mm. A non–rectangular grid was used with a minimum resolution of 24 x 24 pixels. The maximum overlap between adjacent interrogation regions was 50%. Smoke, introduced upstream of the open-loop wind tunnel contraction, was used for seeding. Dual Nd-Yag lasers were used to illuminate a light sheet, placed about 50 mm to the left side of the model centerline (facing upstream).

D. Experimental Uncertainty

The airfoil incidence angles, α's, are accurate to within $\pm 0.03^o$. The LE and TE flap deflection angles are accurate to within $\pm 0.25^o$, C_μ is accurate to within 20% (partly due to slot width uncertainty of ± 0.08 mm and partly due to calibration uncertainties such as sensor location and $\pm 2\%$ uncertainty in hot-wire velocity measurements), and Re_c is accurate to within 3%. The uncertainties of the airfoil integral parameters are listed in Table 2 (in absolute values and related to flow conditions).

Table 2. Uncertainty of Airfoil integral parameters

Parameter	Fully attached	Stalled	Controlled
C_L	0.01	0.04	0.02
C_{dp}	0.002	0.004	0.003
C_D	0.002	0.008	0.006

The large uncertainty in the total drag, C_D, is due to the extrapolation of the wake data for some of the high-lift configurations of the airfoil, to wind tunnel interference, and to uncertainty about wind tunnel static pressure at the wake rake location. It should be noted that the integral parameters in this paper were not corrected for the *significant* tunnel wall interference effects present in the BART facility for the model size used; however, the *relative* improvement in performance is believed to be conservative.

E. Test Conditions (flow and geometry)

The majority of the experiments using the TE flap were conducted at incompressible values of Re_c ranging from 0.24 x 10^6 to 0.75 x 10^6. The flap deflections were varied from $\delta_f = 0^o$ to 60^o for the TE and $\delta_s = 0^o$ to -30^o for the LE.

IV. Results

The baseline (no control) performance of the airfoil is discussed in Reference 8. Some of the relevant baseline data is repeated and discussed here for completeness. The purpose of deflecting the LE flap was to eliminate the possibility of LE separation that supercritical

airfoils are notoriously known for due to the low radius of curvature of the LE.[9] In application, it will be required to consider both large and small LE and TE flap deflections for typical landing and take-off conditions, respectively.

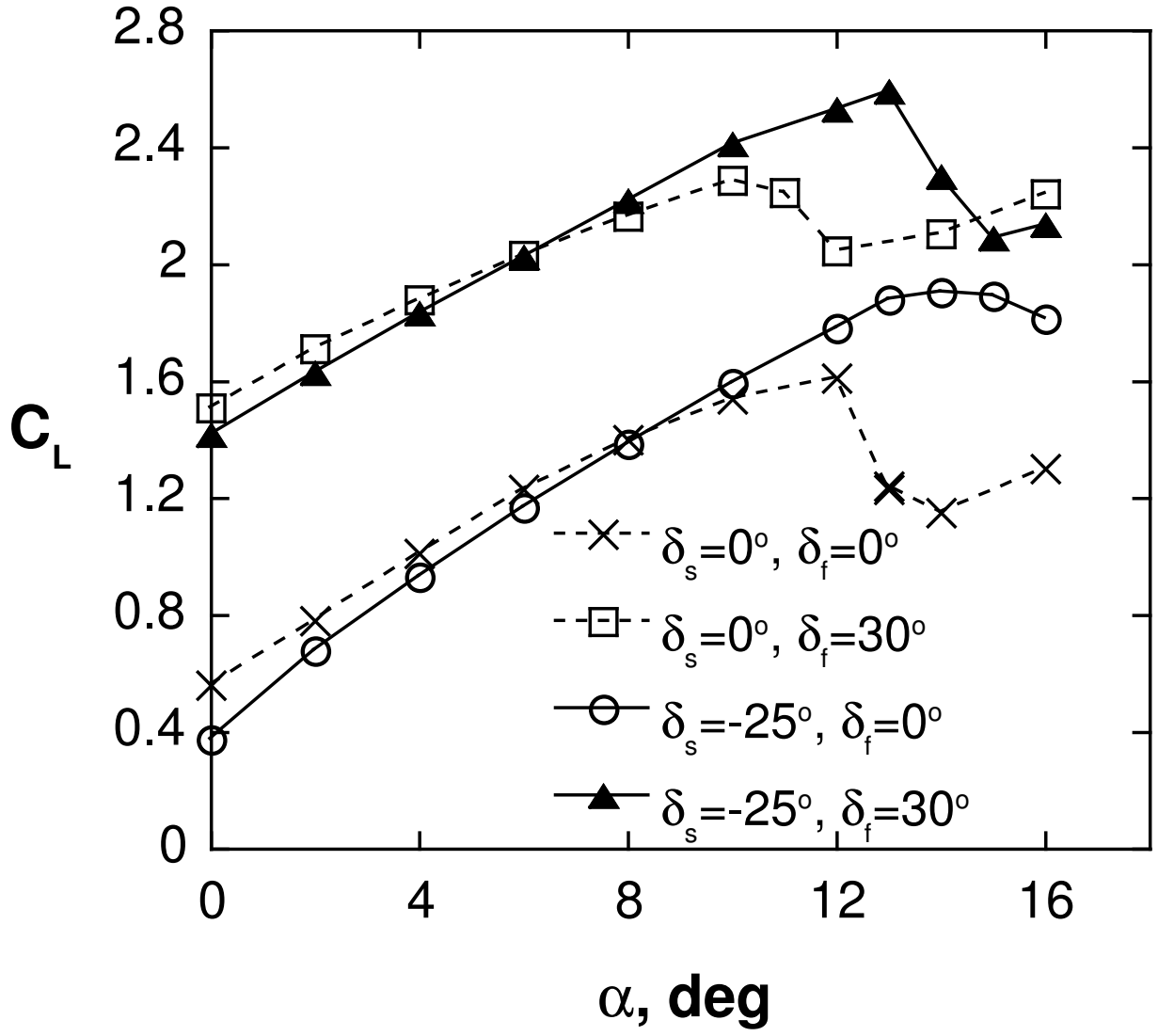

Figure 2. Lift coefficients of the EET airfoil at different high-lift configurations as tested in BART at $Re_c = 0.75x10^6$**.**

Lift data for a candidate landing configuration ($\delta_s = -25^o$ and $\delta_f = 30^o$) are shown in Fig. 2. The following data are also included in this figure: data for the cruise configuration ($\delta_f = \delta_s = 0^o$), data for $\delta_s = -25^o$ at $\delta_f = 0^o$ (showing delayed and milder stall), and data

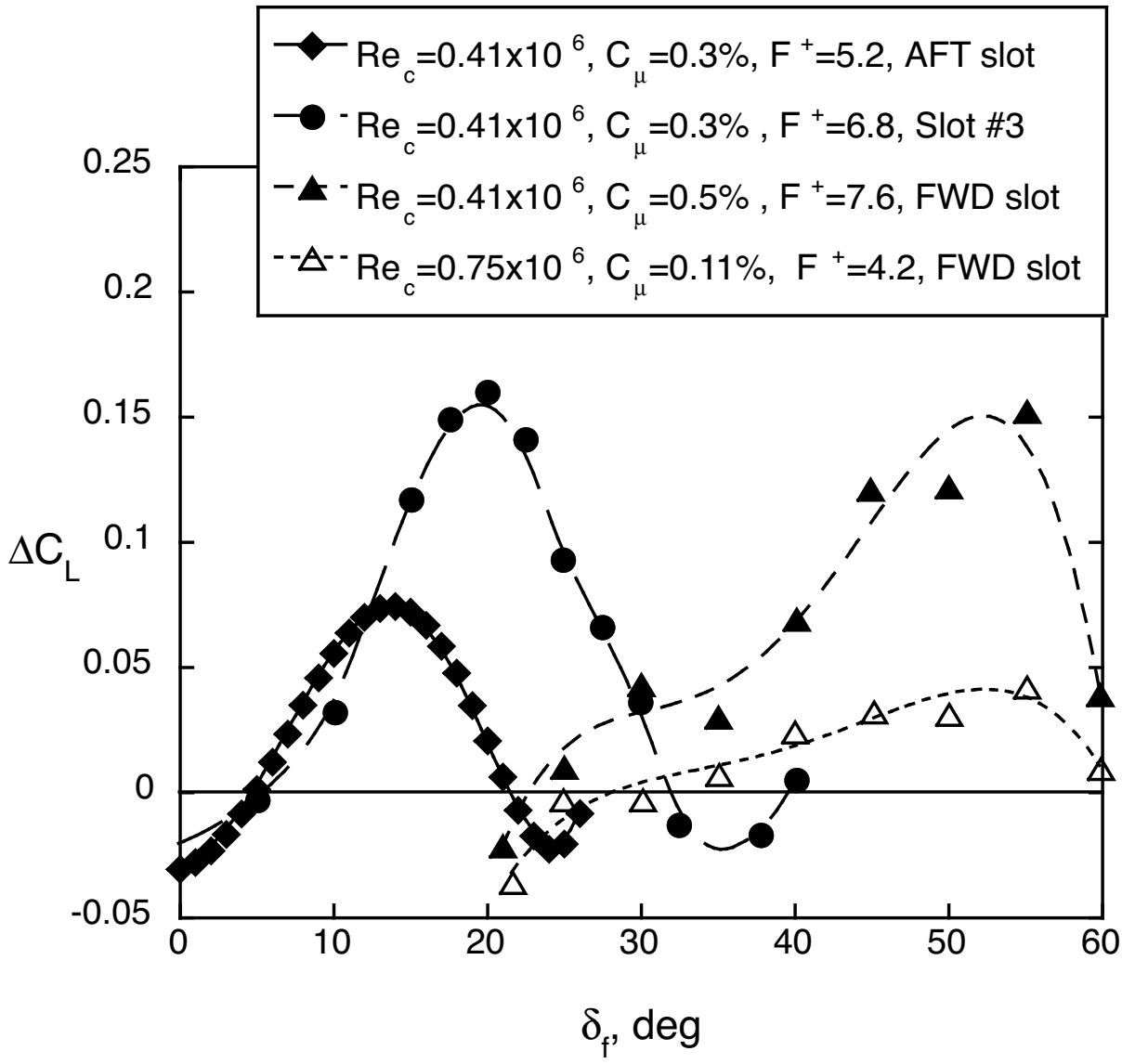

Figure 3. Lift increment vs TE flap deflection angle for different slot locations (shown in Fig. 1(b)). $\alpha = 0^o$, $\delta_s = 0^o$. (Note that AFT slot data are from curve fits of the controlled and baseline data)

for $\delta_f = 30^o$ at $\delta_s = 0^o$ (showing increased lift and earlier, more abrupt stall). The lift data for the $\delta_s = -25^o$ and $\delta_f = 30^o$ configuration indicates that the LE flap effect is almost linearly added to the TE flap effect and its stall milding capability is maintained even at $\delta_f = 30^o$. The challenge is now to apply periodic excitation on both the LE and TE flap shoulders to delay BL separation at both actuator locations allowing larger LE and TE flap deflections and thereby enhanced lift.

A. Effects of the Active TE Flap Excitation Slot Location

A summary of the major findings with regard to the optimal locations for the introduction of periodic excitation, keeping in mind that the aim is increasing the effectiveness of the TE flap, is given in Fig. 3 for $\alpha = 0^o$. In all cases considered, the separating BL was turbulent. The aft slot, located at $x/c = 0.845$ (when $\delta_f = 0^o$), becomes effective for $\delta_f > 5^o$, reaches optimal performance at $\delta_f = 12^o$, and loses its effectiveness at $\delta_f > 20^o$, where the separation point moves upstream of the aft slot. Slot #3, situated roughly 9%c upstream of the aft slot, starts being effective at $\delta_f \approx 10^o$, reaches it peak performance at $\delta_f \approx 20^o$, and stops being effective at $\delta_f > 30^o$, for the same reason as the aft slot. The FWD slot is exposed to the external flow only for $\delta_f > 22^o$ and becomes effective only for $\delta_f > 30^o$, peaks at $\delta_f \approx 50^o$, and losses effectiveness at $\delta_f \approx 60^o$. The effective range of each slot versus δ_f is not significantly sensitive to the C_μ or to F^+ (using $F^+ > 4$) or to Re_c, as shown by the data (Fig. 3). A small adverse effect at the edges of the effective range of each slot is also shown in Fig. 3. Such effects were not seen when using low F^+ excitation or LE excitation, and the source for the current effect is unknown. Note that the small difference in slot locations ($\Delta x/c \approx$3.2%, Fig. 1(b) and Table 1) between the FWD slot and slot #3, results in a 30^o change in δ_f for max effectiveness of the two slots. For comparison the difference between the aft slot and slot #3 ($\Delta x/c \approx$9%) results in only a 3-4^o difference in δ_f for maximum effectiveness. A possible explanation for this significant finding is the curvature in the FWD slot region, while the upper TE flap surface, downstream of slot #3, is almost flat.

B. TE Flap FWD Slot AFC Results

Figure 4(a) shows the lift increment and form–drag alteration due to high F^+, pure sine excitation and amplitude modulation of the F^+=13 excitation at F^+_{AM}=0.32 (Note curve fitted data). The choice of this F^+_{AM} will be explained later. The data of Fig. 4(a) clearly show that larger lift increments are generated between $30^o < \delta_f < 50^o$ when using $F^+_{AM} =$

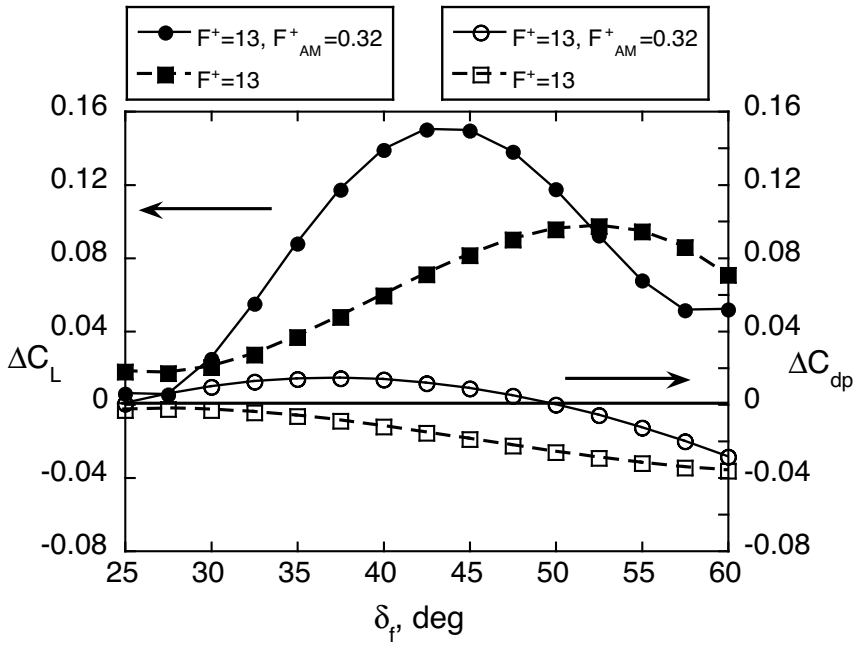

(a) ΔC_L **and** ΔC_{dp} **as a function** δ_f

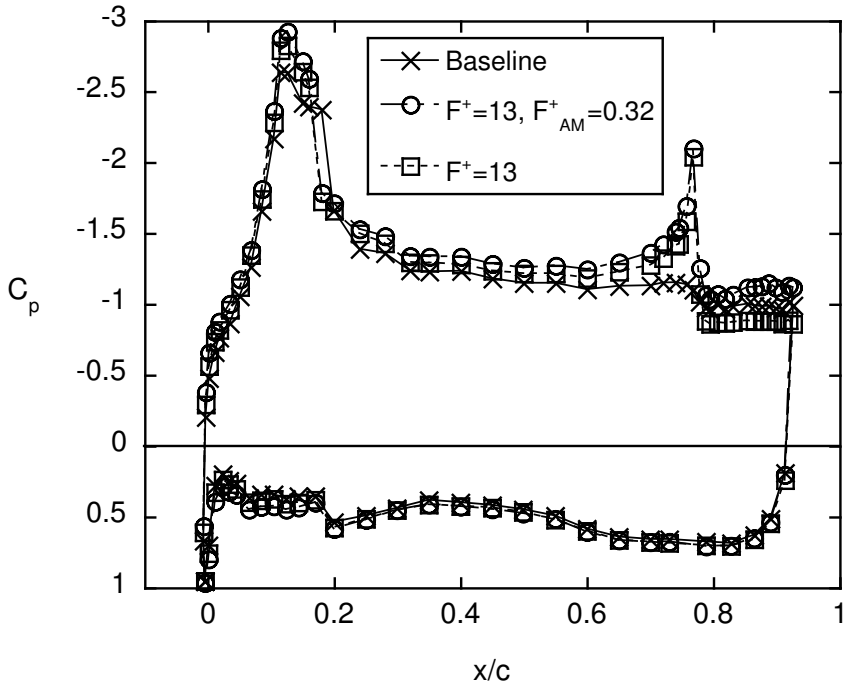

(b) **Pressure Distribution,** $\delta_f = 45^o$

Figure 4. TE Flap FWD Slot Control. Re_c**=0.24x10**$^6, \alpha = 0^o, \delta_s = -25^o, C_\mu$**=0.38%**

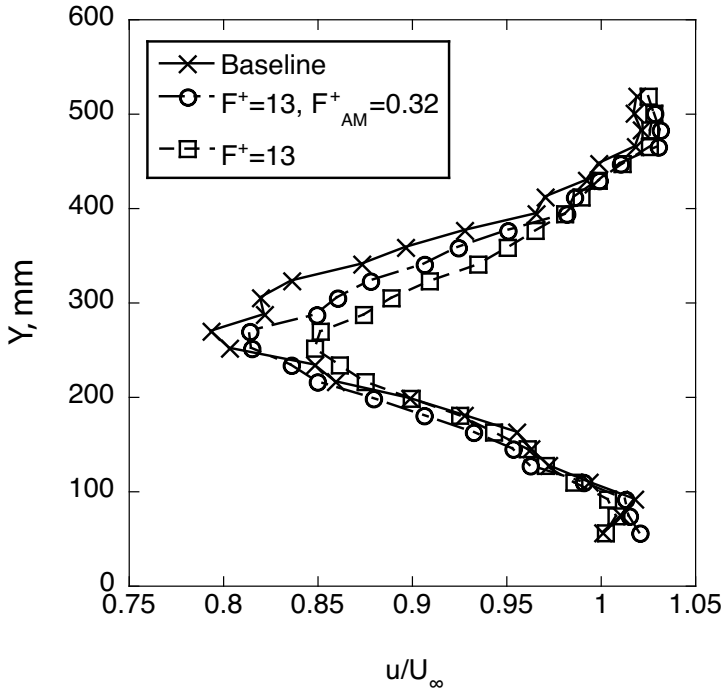

(c) **Wake distribution,** $\delta_f = 45^o$

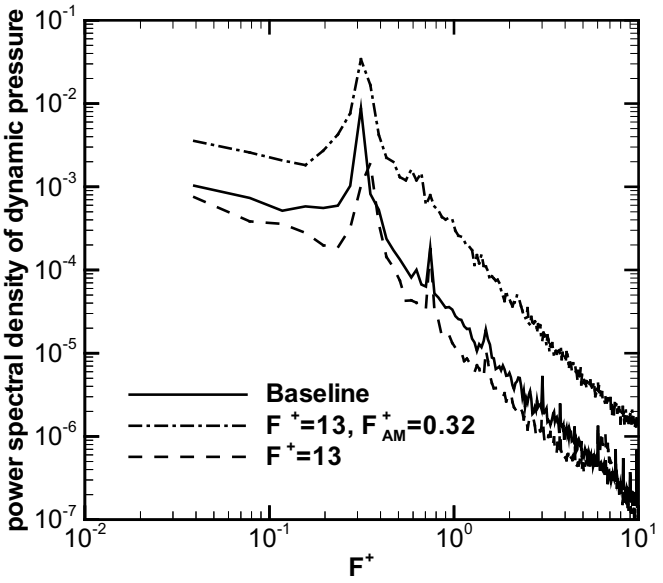

(d) **Flap trailing edge pressure spectra,** $\delta_f = 45^o$

Figure 4. TE Flap FWD Slot Control. Re_c**=0.24x10**$^6, \alpha = 0^o, \delta_s = -25^o, C_\mu$**=0.38%, Cont.**

0.32 rather than using $F^+ = 13$. However, the high F^+ excitation reduces the form drag more effectively throughout the δ_f range. The data further indicate that the longer wave length generated by the $F^+_{AM} = 0.32$ excitation is less sensitive to the curvature of the TE flap surface, reducing the effective δ_f range of the TE flap FWD slot by about 10^o, with respect to the pure sine, high frequency excitation. The application aspect of the above finding is that it should be possible, by changing only the excitation frequency, to alter the lift to drag ratio, while maintaining lift and to obtain similar effects as would be obtained by altering the excitation slot location. These effects hypothesized to be related to the ratio between the convective low F^+_{AM} wave length and the radius of curvature at the excitation slot and the flow separation region.

The increase in form-drag when using the F^+_{AM} excitation may be due to exciting the flow near the natural vortex shedding frequency (VSF). It was recently shown (Naim et al,[10] Naim [11]) that excitation at frequencies close to the natural VSF increases the drag of bluff bodies. This occurs due to closer forming and more energetic von Karman vortices in the wake of the separated bluff body. The combined effect induces a stronger upstream directed flow (in a frame of reference advected with the body), hence larger drag. It remains to be seen if a similar mechanism is active in separated flow over conventional airfoils as well. The natural VSF of the base flow data, described in Fig. 4(b) and Fig. 4(c), can be deduced from the pressure spectra measured at the trailing edge, shown in Fig. 4(d). The data show a distinct peak at $F^+ \approx 0.3$.

The C_p distributions and wake velocity profiles at δ_f=45^o are presented in Figs. 4(b)-4(c) and provide a possible explanation for the effects of the excitation on the C_L and C_{dp}. The data of Fig. 4(b) indicates that the low F^+_{AM} and the high F^+ excitations have the opposite effect on the upper surface TE flap pressures . The average C_p (x/c=0.79 to the TE), on the TE flap, of the baseline flow is -0.984 when low F^+_{AM} excitation is applied the average C_p on the TE flap decreases to -1.097 and when high F^+ excitation is used the average C_p increases to -0.876. The low F^+ excitation generates mostly an upstream effect, that is crucial for the lift increment at high δ_f's, where complete TE flap reattachment is impossible with reasonable C_μ. The larger C_p on the TE flap generated by the high F^+, pure sine wave, excitation is beneficial for drag reduction (Fig. 4(c)). This is attributed to the larger pressure on the negatively sloped TE flap upper surface, indicated by the narrower wake and the slightly higher VSF (Fig. 4(d) $F^+ = 13$). From the available data it seems that the high F^+ excitation delays separation, narrows the wake, increases the VSF and reduces

the form-drag (Figs. 4(b), 4(c), and 4(d)). The AM excitation increases the magnitude of the VSF (Fig. 4(d) closer and stronger vortices as indicated by a stronger spectral peak). The VSF "locks" to the AM F^+ and increases the form drag for $\delta_f \leq 50^o$ (Fig. 4(a)). Note that the total drag, predicted from the wake momentum deficit for the AM data is less reliable due to the low frequency oscillation of the wake flow, as indicated by the TE pressure spectra (Fig. 4(d)).

C. TE Flap Slot #3 AFC Results

The lift increment versus TE flap deflection angle for excitation emanating from slot #3 at $Re_c = 0.24x10^6$ and $0.41x10^6$ is presented in Fig. 5. The data shown in Fig. 5 indicate that Re_c has a weak effect on the optimal δ_f of slot #3 excitation. Also, for approximately triple the value of C_μ, only twice the lift increment is obtainable at the lower Re_c. In Fig. 6, the effect of airfoil angle of attack on optimal δ_f for slot#3 is examined at $Re_c = 0.24x10^6$. The data indicate that the airfoil incidence angle has no effect on the optimal TE flap deflection or on the attainable lift increment when using slot #3 with $\delta_s = -25^o$. This finding is encouraging when attempting to increase $C_{L,max}$ of a high-lift airoil.

1. The Effect of Low F^+ AM Excitation

As already mentioned in the context of Fig. 4, low frequency modulation of the high F^+ excitation increases the lift generating capability of the TE flap flow forcing mechanism, while generally increasing rather than decreasing the form-drag. Detailed AM frequency scans are presented and discussed in this section.

Figure 7 shows the effect of variations in the F^+_{AM} on the lift and form–drag, with excitation introduced from slot #3, using $C_{\mu,AM} = 0.2\%$. The geometry and Reynolds number were $\alpha = 0^o$, $\delta_s = -25^o$, $\delta_f = 20^o$, and $Re_c = 0.24x10^6$), respectively. The AM data is compared to pure sine, high F^+, high C_μ (0.6%) data (plotted as square symbols at F^+_{AM}=0). Note that triple the C_μ using pure sine excitation generates approximately the same variation in lift and form–drag as the optimal low F^+_{AM}. Also, the optimal values of F^+_{AM} are different for the lift increment (without form–drag reduction) and form–drag reduction (at half the lift increment). The optimal reduced AM frequencies are $F^+_{AM} \approx 0.5$ for lift increment and $F^+_{AM} \approx 1$ for form–drag reduction. The F^+ sensitivity data are consistent with the pure harmonic, low frequency scan performed by Seifert et. al[1] for lift increment purposes. The

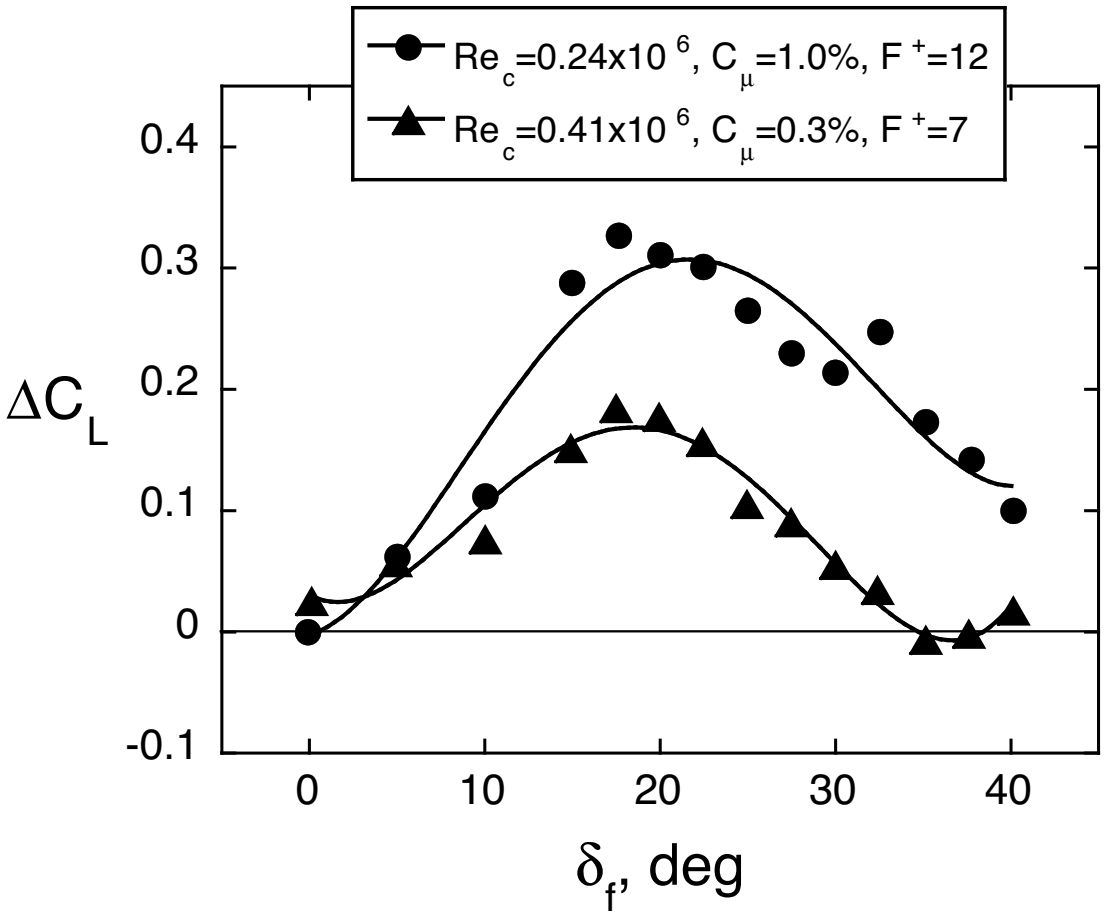

Figure 5. Reynolds number effect on lift increment vs. TE flap deflection angle, $\alpha = 0^o$, $\delta_s = -25^o$, flap slot #3.

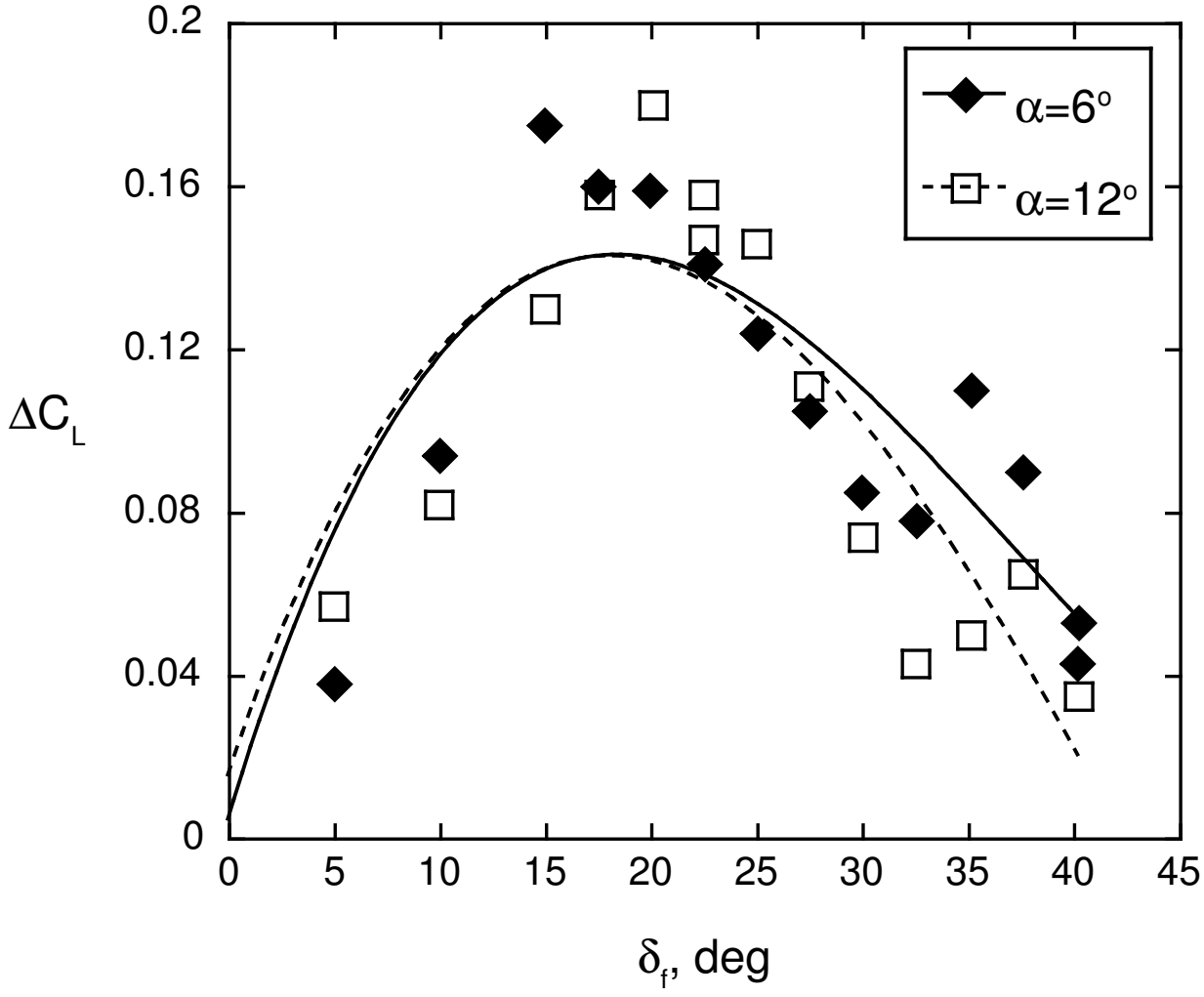

Figure 6. Angle of Attack effect on lift increment vs TE flap deflection angle, $Re_c = 0.24x10^6$**,** $\delta_s = -25^o$**,** $C_\mu = 1.0\%$**, flap slot #3.**

form–drag reduction found at twice the optimal ΔC_L frequency was also observed by Naim et. al.[10,11]

Figure 8 compares the lift increment at $\alpha = 0^o$ and $\alpha = 12^o$ ($C_{L,max}$ of the baseline) with excitation introduced from slot #3. The data indicate, in agreement with Seifert and Pack,[2] that the lift increment is approximately halved (using the same C_μ) when approaching $C_{L,max}$, but the effective F^+_{AM} remains unchanged, though less distinct. The reduction in the effectiveness of the excitation for lift increment is attributed to an increase in the boundary layer thickness, larger adverse pressure gradient on the TE flap, and to the intermittently separated flow at the slot location.

Figure 9(a) shows the lift and Fig. 9(b) shows the form–drag, comparing the effects of the magnitude of the pure sine, high frequency excitation to those due to F^+_{AM}=0.6 excitation. The data shown in Figs. 9 indicate that only a third of the C_μ is required to generate the same increment in lift when using $F^+_{AM} = 0.6$. The form–drag (Fig. 9(b)) initially increases for low levels of C_μ (more significantly for $F^+_{AM} = 0.6$); however, for C_μ >0.15% the trend of the drag data is similar, regardless of the excitation signal frequency content.

Figure 10(a) shows data similar to that of Fig. 9(a), but at a larger incidence angle of $\alpha = 6^o$. The low F^+_{AM} is still more energy efficient, but the form–drag is not increased by using high frequency excitation. It requires, again, roughly only a third the C_μ to generate the same ΔC_L, while drag is not reduced by the available range of C_μ that is deemed incapable of even partial flow reattachment to the TE flap at this α and δ_f. The $F^+ = 12$ excitation and the F^+_{AM} excitation have a similar effect on the C_p distribution upstream of the TE flap shoulder(Fig. 10(b)). When observing the C_p variations due to AFC on the TE flap upper surface, the F^+_{AM} excitation decreases the pressure on the TE flap more than the $F^+ = 12$ excitation, increasing *both* C_L and C_{dp}. The TE flap upper surface average C_p values from x/c=0.8 to the TE are -0.56 for the baseline, -0.62 for the $F^+ = 12, F^+_{AM} = 0.5$ excitation and -0.58 for the $F^+ = 12$ excitation.

D. Flow Details

To better explore flow modifications due to the excitation and correlate these to variations in the BL separation location and eventually to alterations of the aerodynamic performance of the wing in the high-lift configuration, flow physics details need to be studied and understood. For this purpose C_p, hot-film and dynamic pressure data are correlated with flow field data acquired by PIV, as described in Section III, and will be discussed in this section.

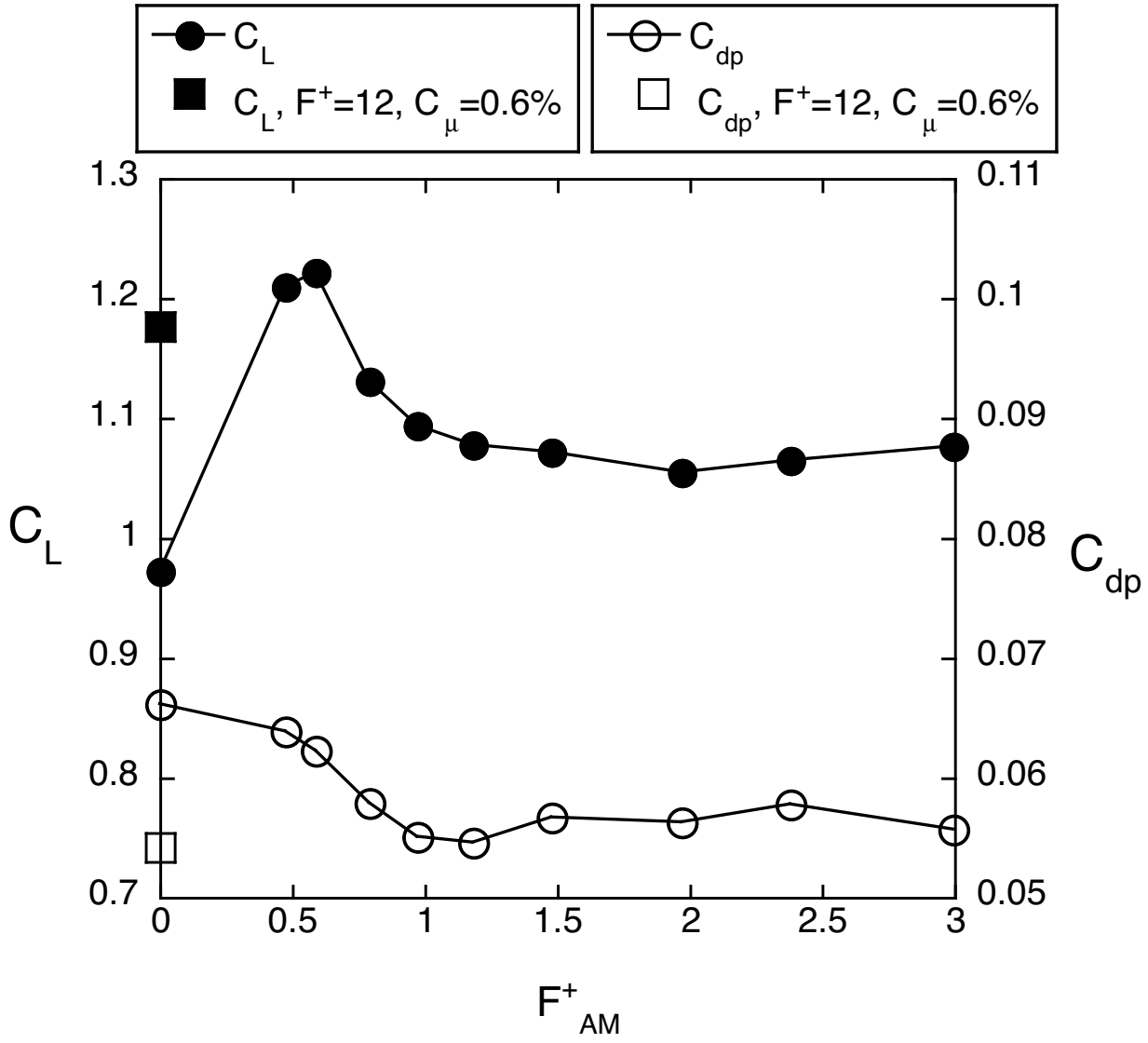

Figure 7. Effect of F^+_{AM} on C_L and C_{dp}, $\alpha = 0^o$, $\delta_s = -25^o$, $\delta_f = 20^o$, flap slot #3 (see fig. 1(b). $Re_c = 0.24x10^6$, C_μ=0.2%.

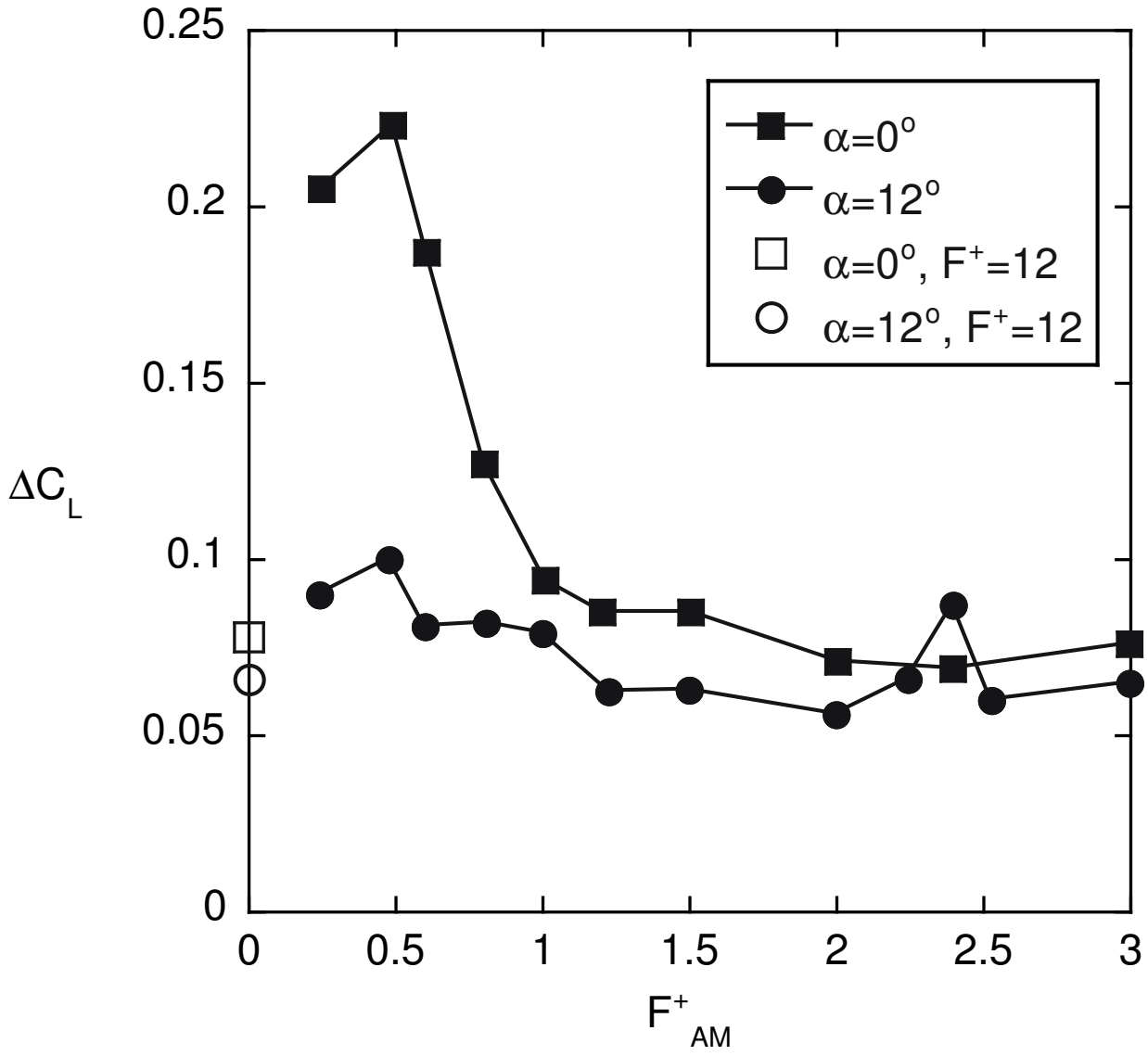

Figure 8. F^+_{AM} **Effect,** $Re_c = 0.24x10^6$**,** $\delta_f = 20^o$**,** $\delta_s = -25^o$**, Flap slot #3,** C_μ**=0.2%.**

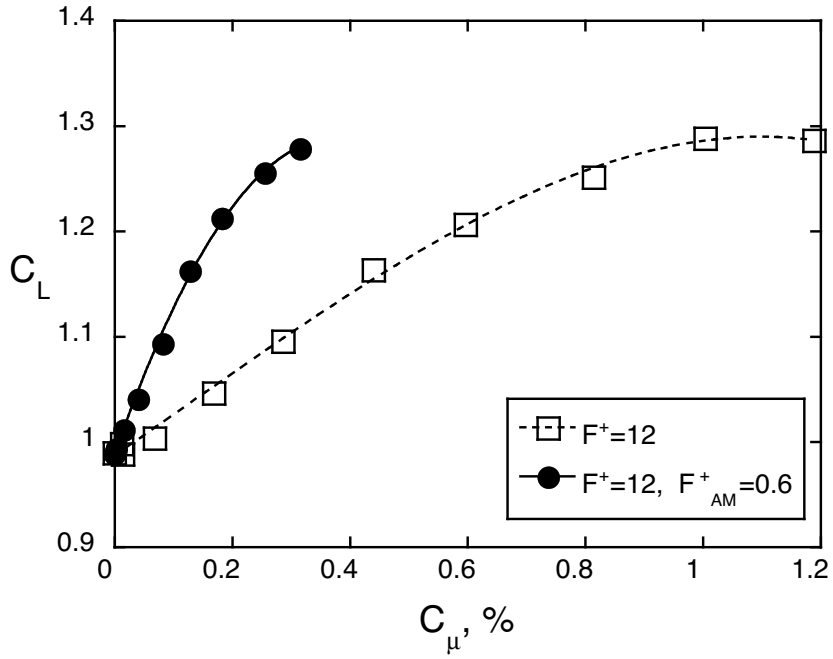

(a) C_μ **effect on** C_L

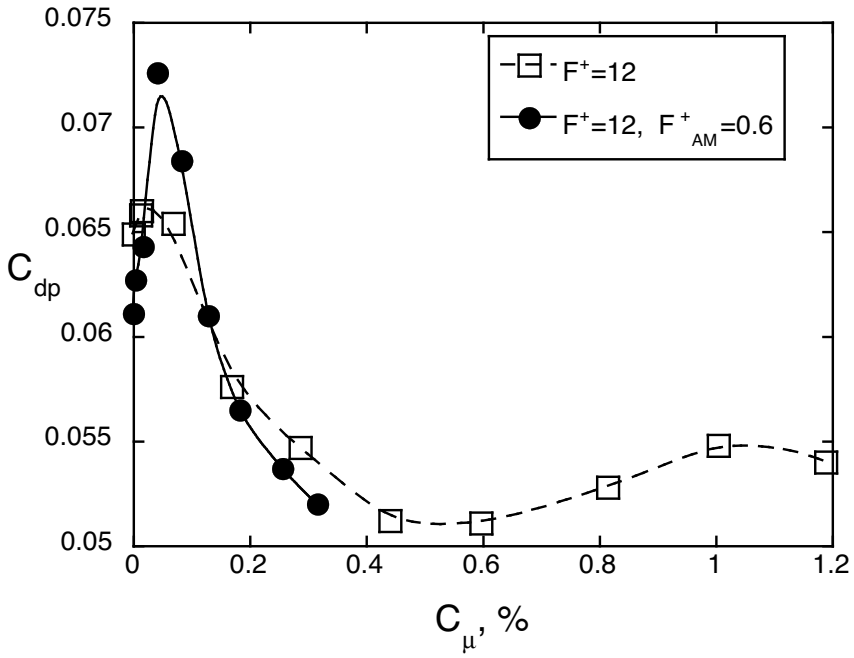

(b) C_μ **effect on** C_{dp}

Figure 9. Amplitude Scan. Flap slot #3, $Re_c = 0.24x10^6$**,** $\delta_s = -25^o$**,** $\delta_f = 20^o, \alpha = 0^o$**.**

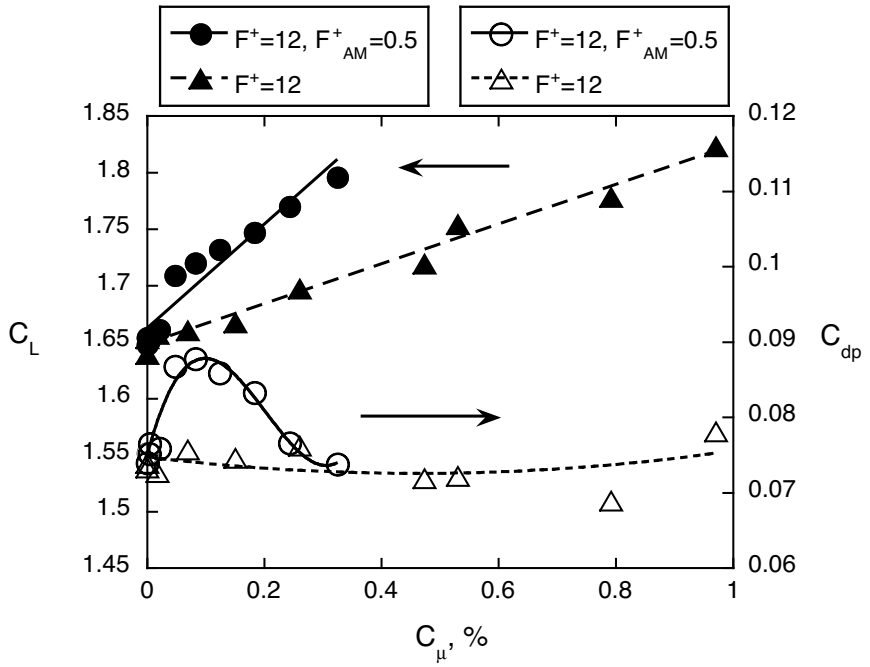

(a) **Effect of Pure Sine control and AM control on C_L and C_{dp}.**

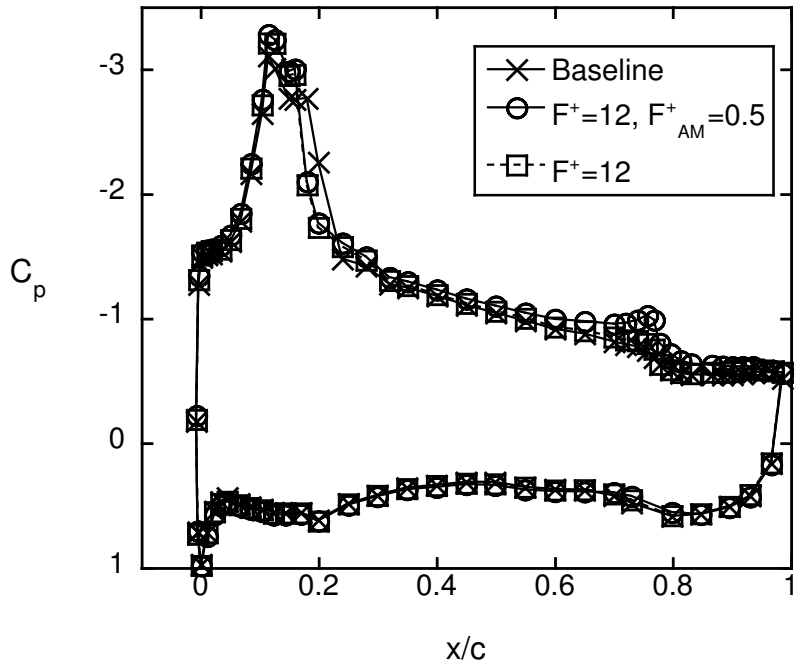

(b) C_p **plot at** $C_\mu \approx 0.08\%$

Figure 10. Amplitude Scan. Flap slot #3, $Re_c = 0.24x10^6$**,** $\alpha = 6^o$**,** $\delta_s = -25^o$**,** $\delta_f = 20^o$**.**

Figure 11(a) shows the C_p distributions of the baseline and F^+=12 controlled flow fields at $\alpha = 6^o$. The excitation is introduced from slot #3 indicated by the vertical, dotted line superimposed on the C_p plot at x/c=0.78 . A strong suction peak was established at the slot and upstream acceleration was induced due to the excitation. The flow on the TE flap is partially reattached resulting in a ΔC_L=0.17 and ΔC_{dp}=0.004 (the excitation increases both C_L and C_{dp} at this condition). The excitation on the TE flap also promotes laminar-turbulent transition on the LE flap. This presumably happens due to the increased circulation over the entire airfoil that generates a more severe adverse pressure gradient or by acoustic radiation from the TE flap excitation to the LE separation bubble. The length of the separation bubble seen at x/c=0.20 in the baseline C_p distribution is reduced (Fig. 11(a)). The dashed box in Fig. 11(a) represents the region where the PIV data was acquired (refer only to the x/c bounds) and these data are presented in Fig. 11(b)-11(c). The PIV data, acquired using two partially overlapping cameras, show that the baseline flow separates from the TE flap at x/c $\approx$ 0.8 (Fig. 11(b)- 11(c)) and the separated streamline flows at an angle of about -10^o with respect to the freestream direction. When excitation from slot #3 is introduced, separation is delayed to x/c$\approx$0.9 and the separating streamline angle is about -23^o. Note that the inclination of the upper surface of the TE flap is about -36^o. The induced upstream acceleration is demonstrated by the reduction in the boundary layer displacement thickness, δ^*, at x/c=0.74 from 6.1 mm in the baseline to 3.3 mm in the controlled flow.

E. Combination of LE and TE Control

To effectively use the potential of the simplified high–lift system, separation should be controlled on both the LE and TE flap shoulders. The role of the LE actuator would be to maintain mostly attached flow on the entire main element, resulting in attached flow at the TE flap slot location. Otherwise, separation would take place upstream of the active slot, voiding its effectiveness, that relies on mixing enhancement. If the separated shear layer is remote from the active slot, communicated only by "dead" air, high momentum fluid can not be transported to the vicinity of the TE flap and its effectiveness would be low. While Reference 8 described the application of AFC to the LE flap shoulder, with the aim of maintaining attached flow on the main element up to $C_{L,max}$, the majority of the current paper was devoted to AFC application on the TE flap upper surface. Effects attributed to curvature, increased BL thickness and larger adverse pressure gradients are significantly complicating AFC application at the TE flap region. Nonetheless, combined LE and TE

flap AFC was attempted at low TE flap deflections where AFC benefits on the TE flap performance persisted to $C_{L,max}$.

Figure 12 shows data combining the LE actuator with the flap actuator. The data presented are at $Re_c = 0.41x10^6$ with $\delta_f = 5^o$ and $\delta_s = -25^o$. Excitation at the LE flap shoulder alone, using F^+=22, is compared to excitation using F^+=22 with F^+_{AM}=4, showing slightly superior results due to the AM excitation. The flap actuator was operated at F^+=5 and excitation was introduced through the AFT slot. In this case, C_μ for the TE flap and LE flap actuators was 0.35% and 0.015%, respectively. Excitation at the LE flap shoulder (x/c=0.14%) using either the pure sine signal or the AM signal, increased $C_{L,max}$ by 0.05 and delayed stall incidence by 2^o. Control applied from the AFT slot of the flap actuator alone increased lift at stall by 0.03, but did not alter the stall angle. Note that typically increasing TE flap effectiveness or loading causes earlier TE flap stall. When the LE and TE excitations were combined, it resulted in similar gains in performance until $\alpha = 14^o$, where $C_{L,max}$ of the baseline was measured. However, the combination of pure sine, high frequency excitation was more effective at larger α, increasing $C_{L,max}$ to 2.1 and delaying stall to 16^o. The larger effect of the high frequency LE excitation combined with the TE excitation might be connected to the absence of large coherent structures generated by the low frequency AM excitation, causing intermittently reversed flow at the the TE flap shoulder location.

V. Summary and Conclusions

Although flow separation from the leading edge could be controlled using relatively low C_μ excitation, controlling separation on the trailing edge flap requires larger periodic momentum input. As was the case when controlling separation at the leading edge, amplitude modulation (AM) of the high frequency excitation reduced the required C_μ. While a 50% reduction in C_μ was measured when using AM excitation at the leading edge, a factor of 3 reduction in C_μ was measured when using AM on the trailing edge flap.

Curvature is believed to play an important role in the separation control process and the ratio between the resulting excitation wavelength and the radius of curvature might be a relevant parameter. The optimal trailing edge flap defection for a particular excitation slot location on the trailing edge flap changed significantly in regions of high curvature. Near the shoulder of the trailing edge flap, where the surface is highly curved, a 3.2% chord change in the slot location caused a 30^o change in the TE flap setting (δ_f) for maximum effectiveness.

While in a region where the TE flap was not highly curved, a change of 9% chord change in the slot location caused only a 3-4^o change in δ_f for maximum effectiveness.

The combination of LE and TE excitations is the primary goal of the research. Preliminary data using combined LE and TE excitations indicates that increased airfoil performance can be obtained when control is applied simultaneously at both locations. LE control with AM excitation was more effective than high frequency pure sine excitation when using the same C_μ. However, when high frequency pure sine excitation at the TE flap was combined with the LE excitation, better performance gains were measured when using high frequency pure sine excitation at the leading edge. The physical understanding of the above finding requires further study.

VI. Acknowledgements

The authors would like to thank the following individuals for their support of the research program, Anna McGowan, William Sellers, Michael Walsh, Anthony Washburn, Luther Jenkins, John Lin, Norman Schaeffler, Richard White, George Hilton, Johnny Mau, Louis Hartzheim, Susan Palmer, and R. David Lewis.

References

[1]Seifert, A., Darabi, A., and Wygnanski, I., "On the Delay of Airfoil Stall by Periodic Excitation," *Journal of Aircraft*, Vol. 33, No. 4, 1996, pp. 691–699.

[2]Seifert, A. and Pack, L. G., "Oscillatory Control of Separation at High Reynolds Numbers," *AIAA Journal*, Vol. 37, No. 9, 1999, pp. 1062–1071.

[3]Seifert, A. and Pack, L. G., "Active Flow Separation Control on Wall-Mounted Hump at High Reynolds Numbers," *AIAA Journal*, Vol. 40, No. 7, 2002, pp. 1363–1372.

[4]McClean, J. D., Crouch, J. D., Stoner, R. C., Sakurai, S., Feifel, G. E., Feifel, W. M., and Rush, H. M., "Study of the Application of Separation Control by Unsteady Excitation to Civil Transport Aircraft," NASA/CR 1999–209338, 1999.

[5]Lin, J. C. and Dominik, C. J., "Parametric Investigation of a High–Lift Airfoil at High Reynolds Numbers," *Journal of Aircraft*, Vol. 34, No. 4, 1997, pp. 485–491.

[6]G.V.Lachmann, *Boundary Layer and Flow Control, Vol. 1*, Pergamon Press Inc., 1961.

[7]Margalit, S., Greenblatt, D., Seifert, A., and Wygnanski, I., "Active Flow Control of a Delta Wing at High Incidence using Segmented Piezoelectric Actuators," AIAA Paper 2002–3270, June 2002, Accepted for Publication, Journal of Aircraft, April 2004.

[8]Pack, L. G., Schaeffler, N. W., Yao, C., and Seifert, A., "Active Control of Separation from the Slat Shoulder of a Supercritical Airfoil," AIAA Paper 2002–3156, June 2002.

[9]Abbott, I. H. and van Doenhoff, A., *Theory of Wing Sections*, Dover Publications, 1949.

[10]Naim, A., Greenblatt, D., Seifert, A., and Wygnanski, I., "Active Control of Cylinder Flow with and without a Splitter Plate using Piezoelectric Actuators," AIAA Paper 2002–3070, June 2002.

[11]Naim, A., *Active Control of Cylinder Flow with and without a Splitter Plate*, Master's thesis, Dep. of Fluid Mech. and Heat Transfer, Faculty of Engineering, Tel-Aviv University, Israel, March 2003.

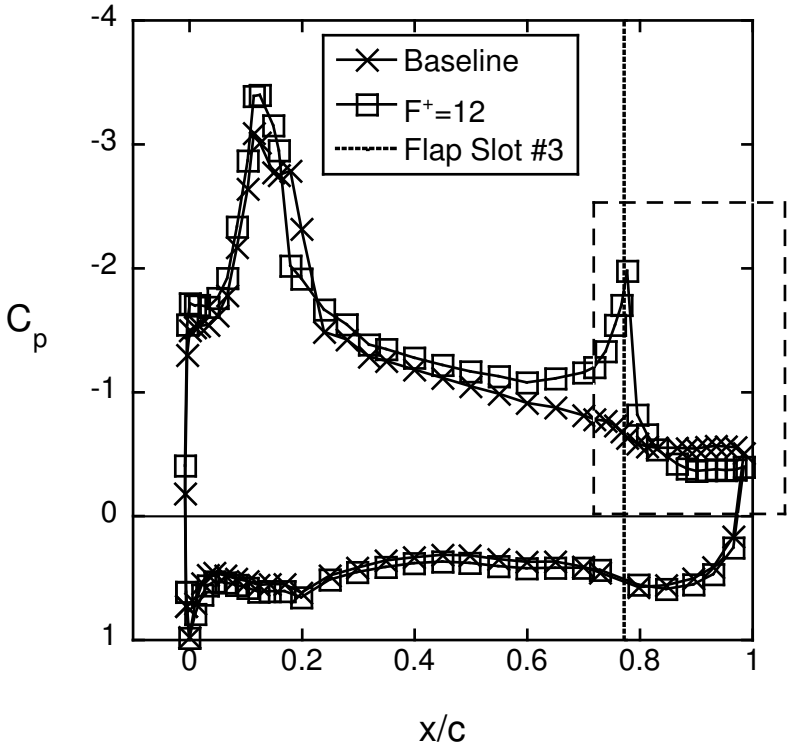

(a) C_p **distribution**

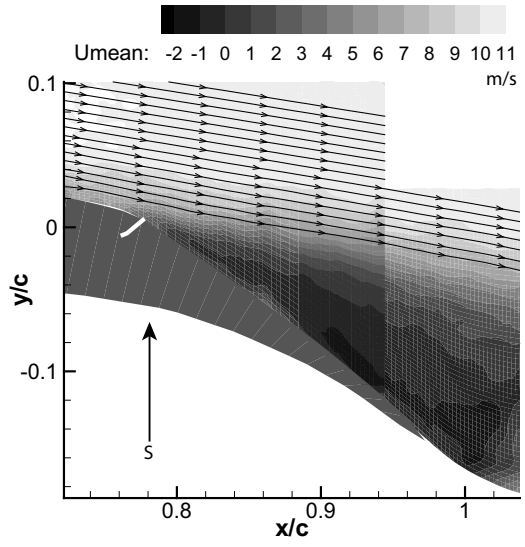

(b) **PIV Baseline**

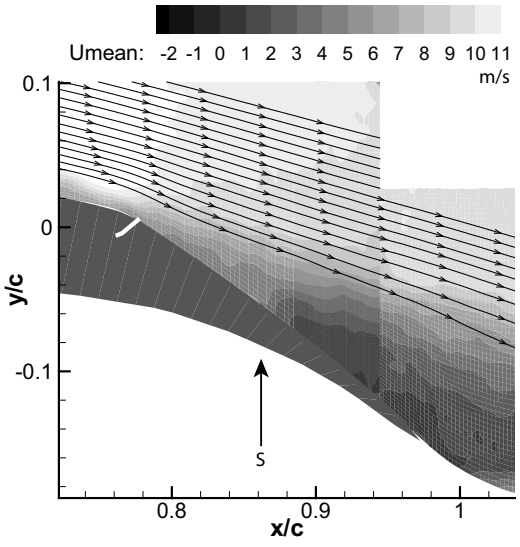

(c) **PIV Controlled,** F^+**=12,** C_μ**=1.0%**

Figure 11. Baseline and controlled flow field. $Re_c = 0.24x10^6, \alpha = 6^o, \delta_s = -25^o, \delta_f = 20^o$**,** F^+**=12,** C_μ**=2.4%. Arrows shown in PIV images indicate x/c location of separation on upper surface of model.**

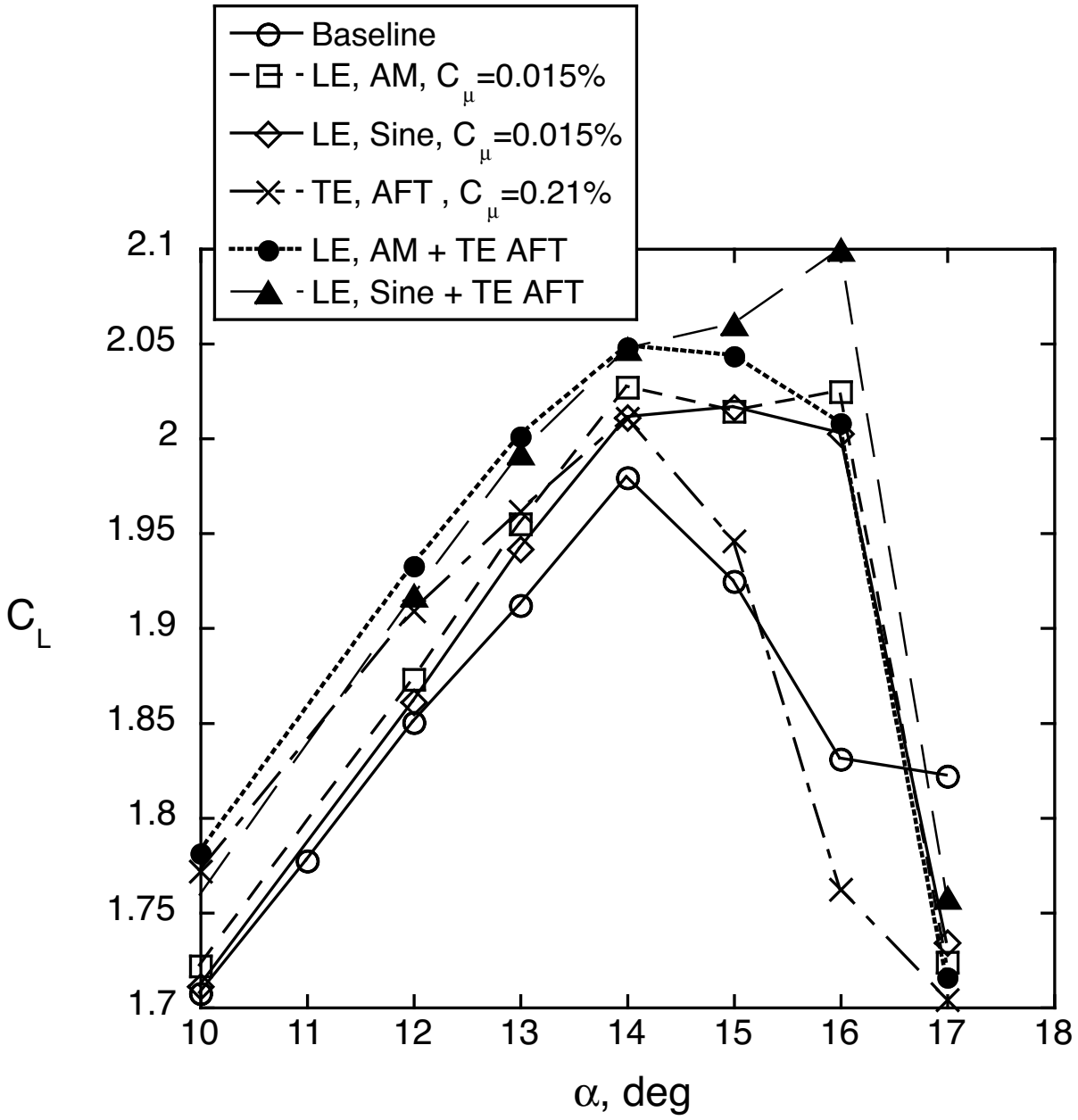

Figure 12. Effect of LE and TE flap control on C_L. $Re_c = 0.41x10^6$, $\delta_f = 5^o$, $\delta_s = -25^o$, F^+_{LE}**=22,** $F^+_{AM,LE}$**=4,** F^+_{TE}**=5.**